



# A novel current controller design for grid-integrated PV inverter system

Ayaz Ahmad<sup>1</sup> · L. Rajaji<sup>2</sup> · A. Iqbal<sup>3</sup>Received: 14 September 2020 / Accepted: 28 January 2021 / Published online: 15 February 2021  
© The Author(s) 2021 

## Abstract

Distributed generators are playing a vital role in supporting the grid in ever-increasing energy demands. Grid code regulation must be followed when integrating the photovoltaic inverter system to the grid. The paper investigates and analyzes a controller model for grid-connected PV inverters to inject sinusoidal current to the grid with minimum distortion. To achieve better tracking and disturbance rejection, a DSP-based current controller is designed with LCL filter. The controller gets the current feedback from the grid, compares it with reference current, and calculates duty cycle to generate PWM pulses to trigger H-bridge converters. The grid voltage is loaded to the initial value in proposed PR controller to ensure the initial inverter voltage to match the grid voltage. The paper presents a novel current controller algorithm for grid-connected inverter system, and simulation is done. A detailed analysis has been carried out to validate the proposed design algorithm. Experimental implementation of the current controller in the DC/AC converter circuits with an LCL filter is done for 5.4 kW to validate and match the simulation model.

**Keywords** CCA · DC/AC · DC/DC · PWM · PR

## 1 Introduction

Better technology, reduced cost, and efficient system are encouraging greening the grid. In the present time, distributed generators are inevitably integrated with the utility grid to meet the increasing power demands. The integration of such a generator must follow the grid code requirement to give and take power from the grid.

Solar inverter system comprises an array of solar panels, DC/DC converter, and DC/AC converter, and both are coupled with the help of DC link capacitor as shown in Fig. 1.

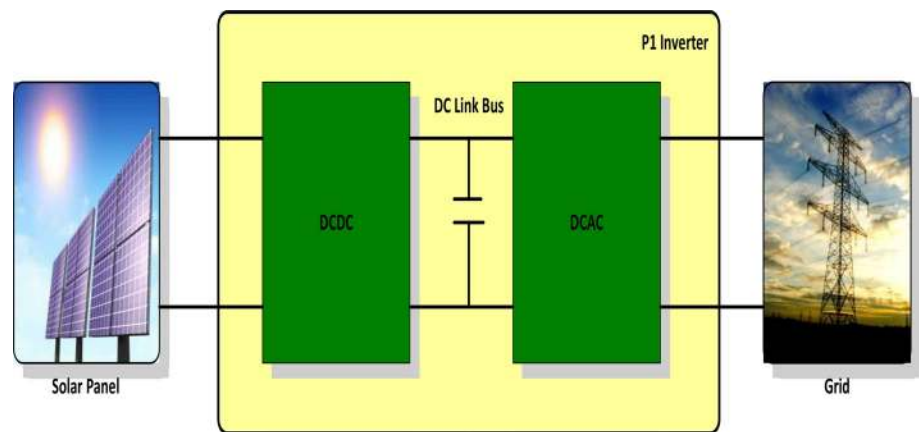
This solar inverter is connected to the power utility grid system through LCL filters. Output ac power is filtered by the LCL filter to mitigate the harmonics and feed to the grid. Current control strategies play a vital role in the performance of distributed solar power system. An

overview of power converters and their various topologies is depicted in [1]. A comparative study is being carried out for PI and PR controller by [2, 3]. Inverters in distributed power generation (DG) systems include dc–ac conversion, output power quality assurance, various protection mechanisms, and system controls [4]. To compensate the grid harmonics and provide disturbance rejection capability, stationary-frame generalized integrators are used to control the fundamental current [5]. A low-cost grid-connected residential scheme is suggested in [6] based on dynamic voltage or current error signals activating a PI controller. Another controller used is low-pass filter in the feedback path along with harmonic compensator to improve the grid current quality [7]. Proportional resonant (PR) controller is an algorithm used in the current controller which is used to integrate the PV inverter into the grid.

✉ Ayaz Ahmad, ayazahmad2000@gmail.com | <sup>1</sup>Department of Engineering, University of Technology and Applied Science, Ibra, Oman. <sup>2</sup>Department of Electrical Engineering, ARM College of Engineering and Technology, Chennai, India. <sup>3</sup>Department of Electrical Engineering, Qatar University, Doha, Qatar.



**Fig. 1** A grid-tied solar inverter system



A repetitive control strategy is implemented to claim a superior tracking and harmonic rejection capability by applying mu synthesis principle [8]. Detailed investigation on power control and current control strategies has been elaborated in [9–12]. Various control algorithms are presented for active and reactive power control when PV inverters are connected to the grid as given by [13–16]. An improved DSP-based controller with predictive and fuzzy logic-based current controller is investigated in [17]. The contribution of power electronics on the efficiency improvement and current harmonics reduction in the grid-connected photovoltaic system is described in [18–21]. The transformerless PV inverter is explained, to minimize the DC component on the injected AC current [22]. Various control strategies, optimization techniques, and analysis have been investigated to implement current control algorithms [23–28]. A comprehensive design methodology of PR controller with zero steady-state error for single-phase grid-connected system is presented by [29]. This paper proposes a novel design and modeling of the current controller for single-phase grid-connected inverter system. The main functional blocks are shown in Fig. 2.

## 2 Proposed current controller for DC/AC module

The current controller algorithm (CCA) is part of the DC/AC Module. The current controller reads the grid voltage, phase, frequency, and generates the electrical power based on the solar panel input power and DC link voltage. Inverter power is fed to the grid in phase with the grid voltage. The proposed current controller comprises zero crossing detector for phase and frequency of the grid voltage. Reference current calculation is done to deliver maximum

available power to the grid. The instantaneous reference current is generated using the reference current sine wave generator. The current delivered to the grid is measured through feedback. PR controller is used to compute PWM duty cycle from the error current.

## 3 Modeling and simulation of current controller

The current controller is the critical functionality of the DC/AC module and is executed for every sample time  $T_s$ . The Simulink model of the current controller is shown in Fig. 3. In this model, the current reference calculation is done for every half cycle that is used for generation of instantaneous reference current sine wave. So, generated instantaneous current sine wave is compared with the feedback current, and error is fed to the PR controller. The output of the PR controller is decoupled with UDC by dividing the URegCC value with UDC link voltage. The current controller outputs the PWM duty cycle value in the range of 0–65, 535 in each direction of the sine wave.

The current reference offset in current reference generation is not used in the model and grid resistance compensation is not included in the model.

Zero crossing detector (ZCD) detects the zero crossings of grid voltage measured at Point of Common Coupling (PCC). ZCD executes every sample time,  $T_s$ . Input samples are downsized by  $5 \cdot T_s$  and select the median value out of 3 successive inputs. The predictive FIR filter is a digital filter to predict the next sample from the previous consecutive 11 inputs. The output of the predictive FIR filter is interpolated to get 4 intermediate samples. The interpolated samples are verified for the zero crossing and the corresponding cycle time is used for computing the grid frequency. The output of the ZCD is shown in Fig. 4. The number of

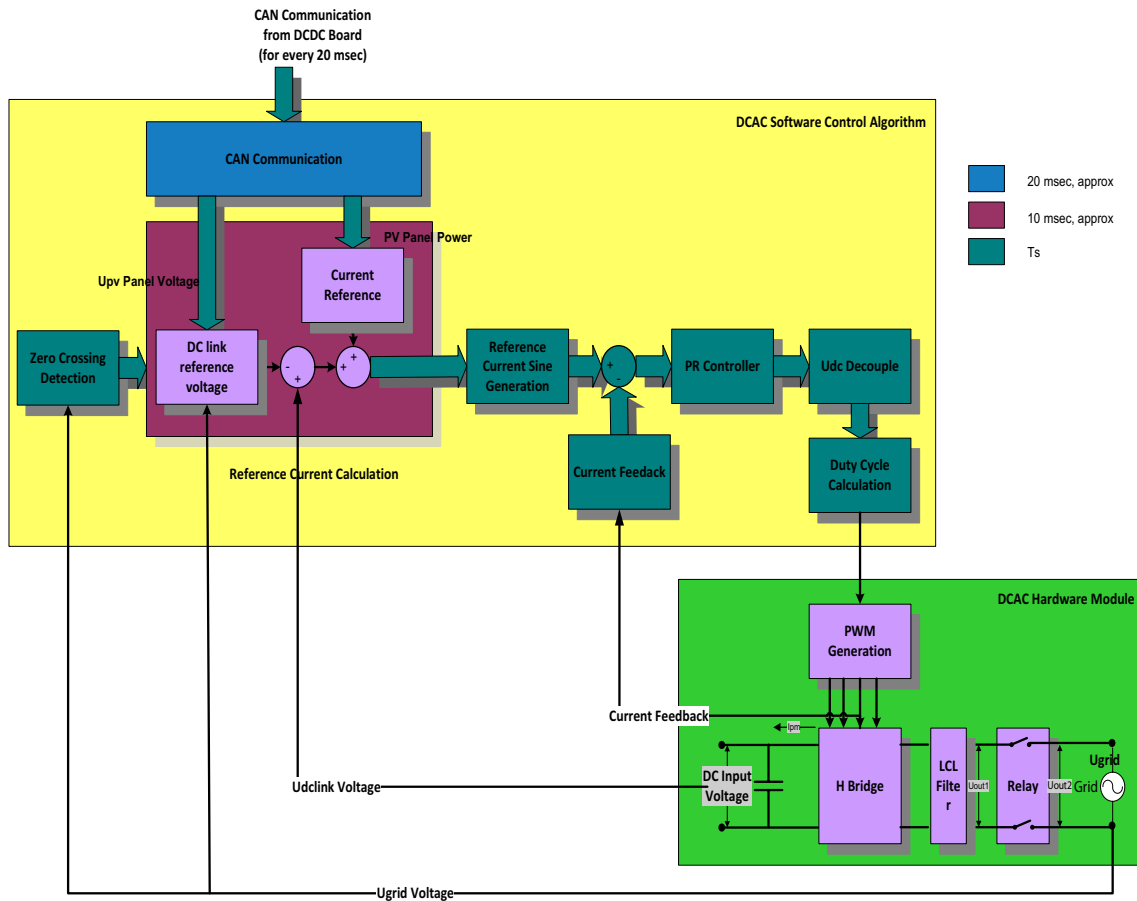


Fig. 2 Functional block of inverter with current controller

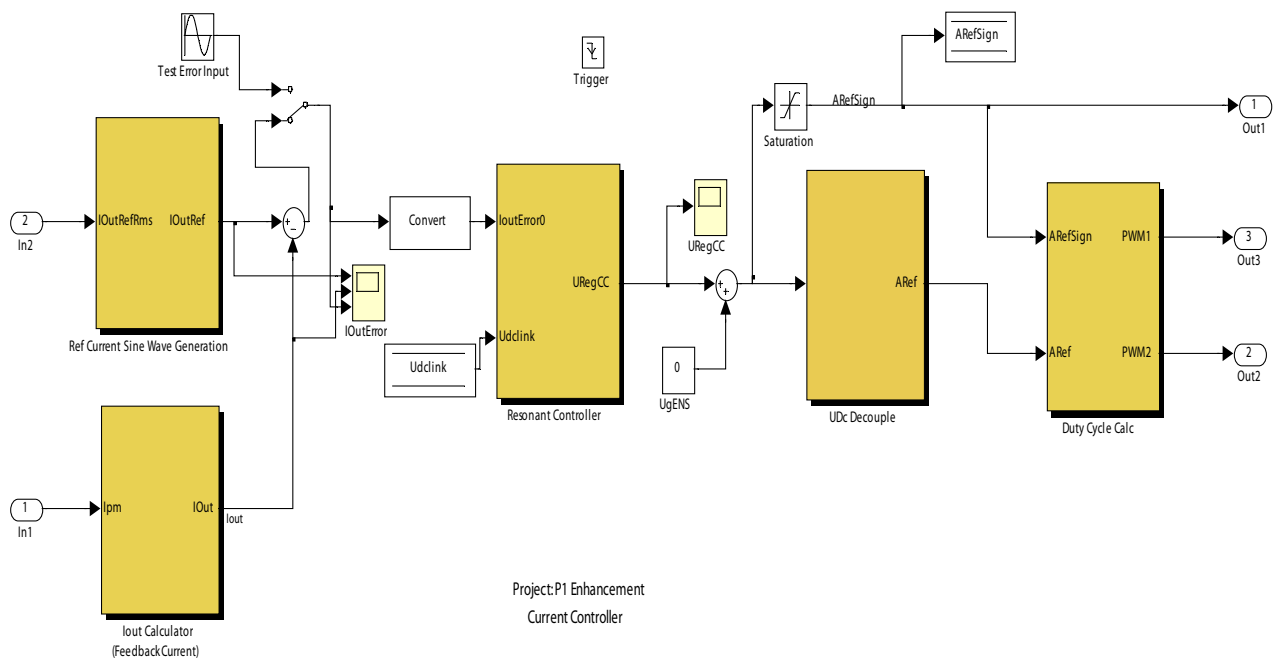


Fig. 3 Current controller model

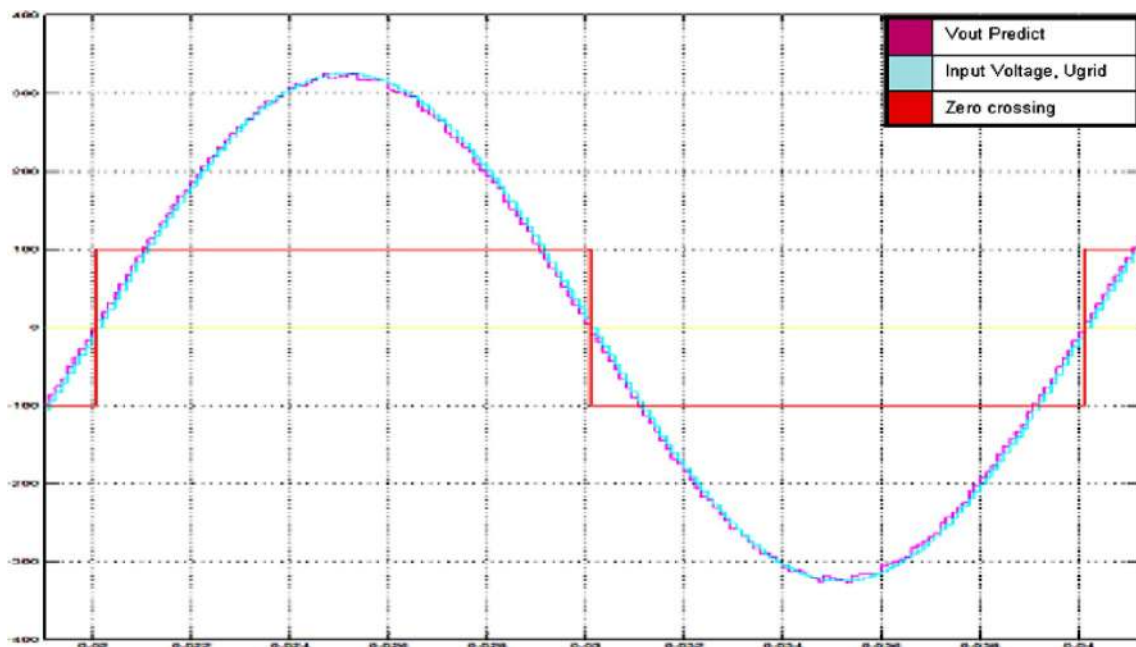


Fig. 4 Output of ZCD

samples for every cycle is fixed as 170. The minor variation in grid frequency is handled by changing the sampling time. For every grid voltage cycle, the new sampling time is manipulated.

$$\text{SamplingTime, } T_s = \text{GridFrequency} / 170.$$

The RMS value of the reference current is calculated for every half cycle of grid voltage. Panel power (Ppv) from DC/DC board through CAN communication, DC link voltage (Udlink), grid voltage (Ugrid) are used for computing current reference (IoutRefRMS) in current controller algorithm.

Feedback current for the current controller is measured from the negative H-bridge of the DC/AC switching circuit. Current in the negative H-bridge is discontinuous DC because of PWM switching. There is no filter involved in the feedback measuring circuit and it is mandatory to sample the current in the middle of the PWM duty cycle to ensure the average current measurement for each PWM pulse. This synchronization of current ADC and H-bridge PWM is available in the DSP processor and explicitly brought out in the Matlab model. The sampled current is converted to sinusoidal wave by considering the polarity of the grid voltage and thus represents the current feedback to the current controller of the inverter. This current feedback is compared with the current reference to compute the

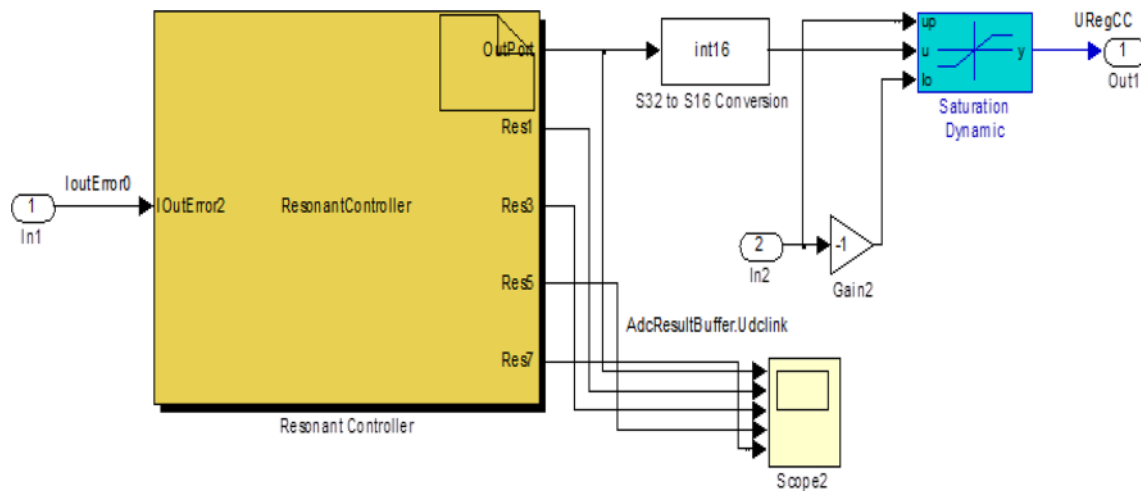
current error. This current error from reference is given as input to the PR controller.

PR controller is the inner loop controller, the output is based on the error current value, that means it estimates the output voltage along with the harmonic compensators. It has 1st, 3rd, 5th, and 7th harmonic compensators with a frequency of 50 Hz, 150 Hz, 250 Hz, and 350 Hz, respectively. Based on the current error value, the highest frequency of the resonant controller will be chosen. Modeling of proportional resonant (PR) controller is shown in Fig. 5.

PR controller block has the advantage of visualizing the outputs of each harmonic compensator. Harmonic components HC5 and Harmonics components HC7 are subjected to anti-windup to limit the peak output. PR controller is discretized using the Backward and Backward Euler method and used in the discretized method as can be seen from Eq. 1.

$$\text{Harmonic Compensator } R_b \& b(Z) = \frac{T_s(1 - Z^{-1})}{1 + (\omega_0^2 T_s^2 - 2)Z^{-1} + Z^{-2}} \tag{1}$$

In Fig. 6, the outputs of each harmonic compensator are probed. From Fig. 6, it is observed that the amplitude of fundamental frequency is much higher than the 3rd, 5th, and 7th order frequencies.



PR Controller  
Project: P1 Enhancement

Fig. 5 PR controller

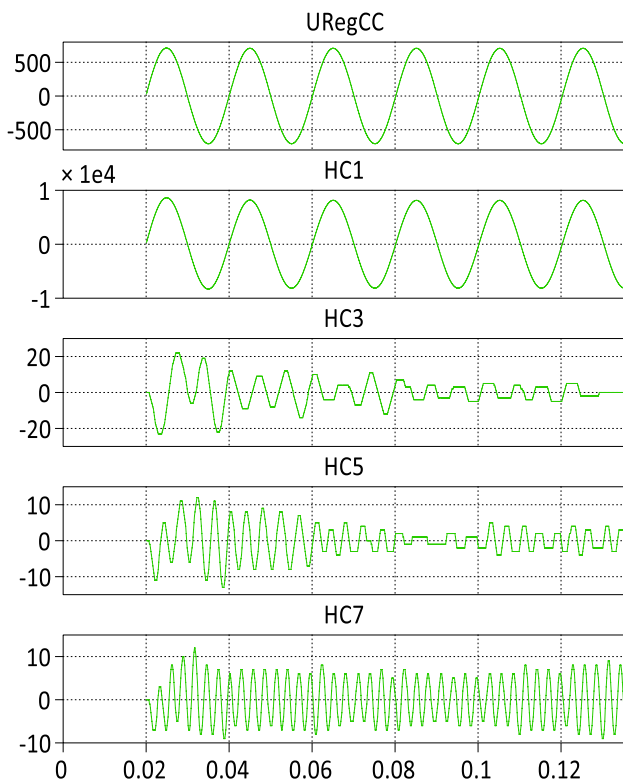


Fig. 6 Output of PR controller

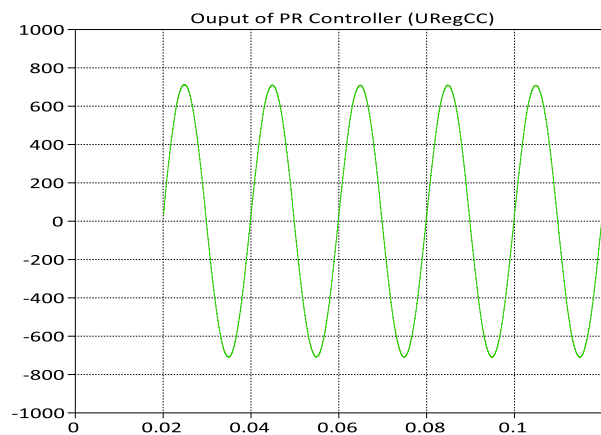


Fig. 7 Consolidated output of PR controller

DC link voltage is decoupled from PR controller output by dividing the PR controller output by DC link voltage.

Figure 7 shows the cumulative output of the proportional controller and Harmonic compensators (HC1, HC3, HC5, and HC7).

DSP calculates the duty cycle from the CCA and generates PWM pulses to trigger the H-bridge gate as shown

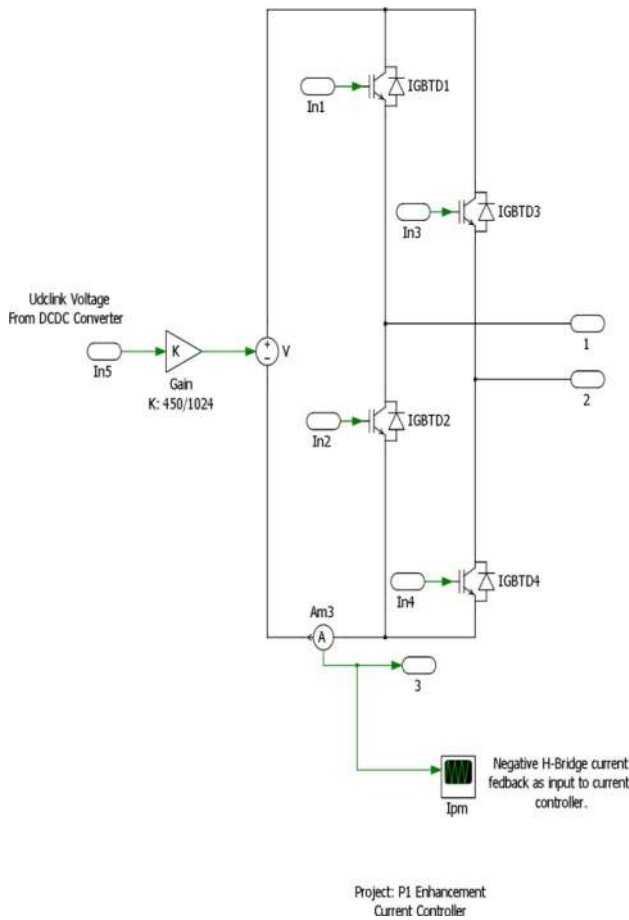
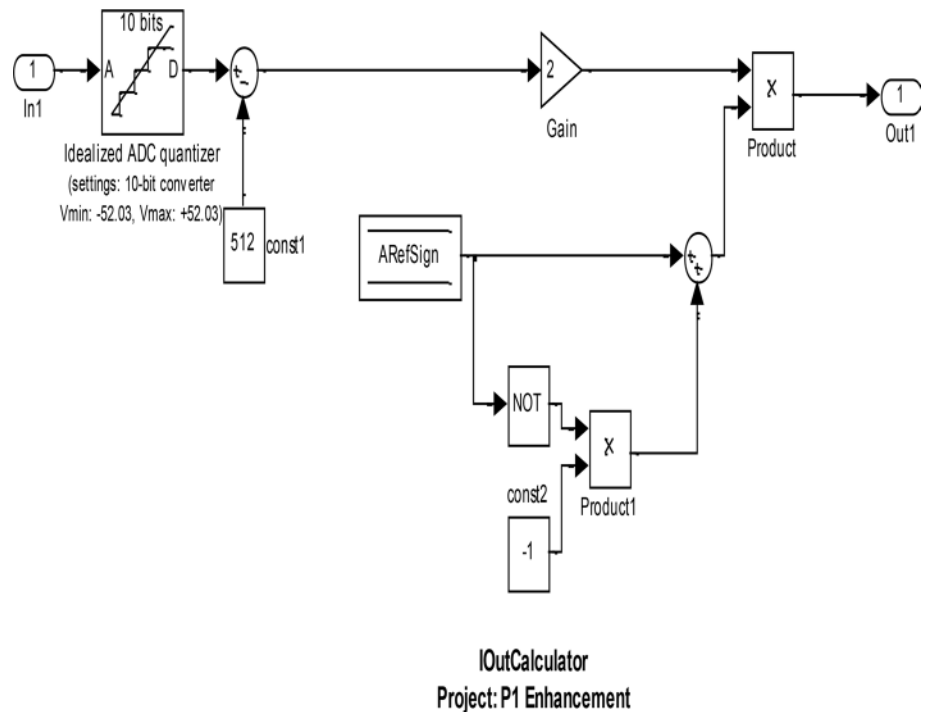


Fig. 8 H-bridge circuit in PLECS

Fig. 9 ADC quantizer for feedback current



in Fig. 8. DC link voltage source forms DC input to the H-bridge.

PWM carrier frequency is twice as that of the sampling frequency. For every sampling time (8.5 kHz approx.), the current control algorithm computes the duty cycle based on the error current and generates PWM pulses of 17 kHz. Zero crossing detection calculates frequency for every period (grid voltage) and this decides the PWM frequency for the next cycle.

Feedback current sensor is mounted on the negative H-bridge. Feedback current is discontinuous and there is no filter available in the current sensor measuring circuit. DSP is expected to read feedback current when the PWM gate is switched ON and also at the mid of the PWM pulse to ensure the read value is average feedback current. Feedback current is measured in mid of the second PWM pulse. Time delay of  $0.75 \cdot T_s$  is involved in reading the feedback current from the PWM output.

Feedback current is calculated by ADC quantizer as shown in Fig. 9. Feedback current module samples the current in the mid of the PWM pulse on negative H-bridge. The sampled current is quantized as 10-bit values in the scale of -52.03A to +52.03 A (for 5.4 kW). Figure 10 shows the current input and current output of the feedback current module. Since the current is measured in the negative H-bridge, the current is unidirectional, and sign conversion is required for the negative cycle of the sine wave.

Figure 11 illustrates the reference current, feedback current, and the error current. Table 1 shows the time-domain



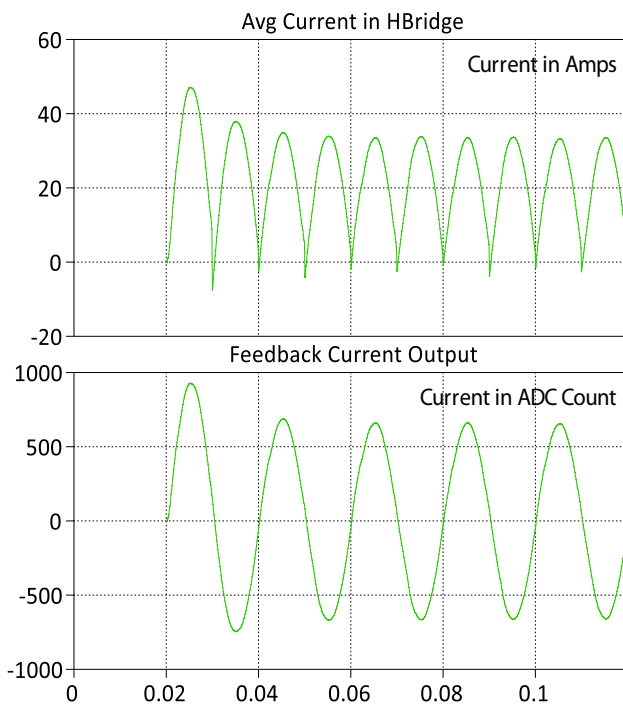


Fig. 10 Input and output of current feedback

characteristics of the error current. The error current is high for the first cycle and in steady state, the average error reads out  $9 \times 52.03 / 1024 = 457$  mA (Scaling + 52.03A—1024). Figure 12 shows the feedback current measured at the negative H-bridge, the input side of the inverter circuit. From this current, the average current is estimated, and feedback current is calculated.

The average current along with feedback current is shown in Fig. 13.

Figure 14 explains how the average current sampled at mid of PWM pulse width and then it is fed back as current feedback signal to the current controller.

LCL filter is connected across the inverter output to filter out the current harmonics while power flows from inverter to power grid. Figure 15 shows the power circuit of the LCL filter. The current control loop of the LCL filter is shown in Fig. 16.

LCL filter circuit parameters are detailed in Table 2

### 4 Simulation results

When relay connects the inverter to the grid, the initial inverter voltage is set based on the previous half cycle of grid voltage as shown in Fig. 17. The grid voltage is loaded to the initial value in PR controller to ensure the initial

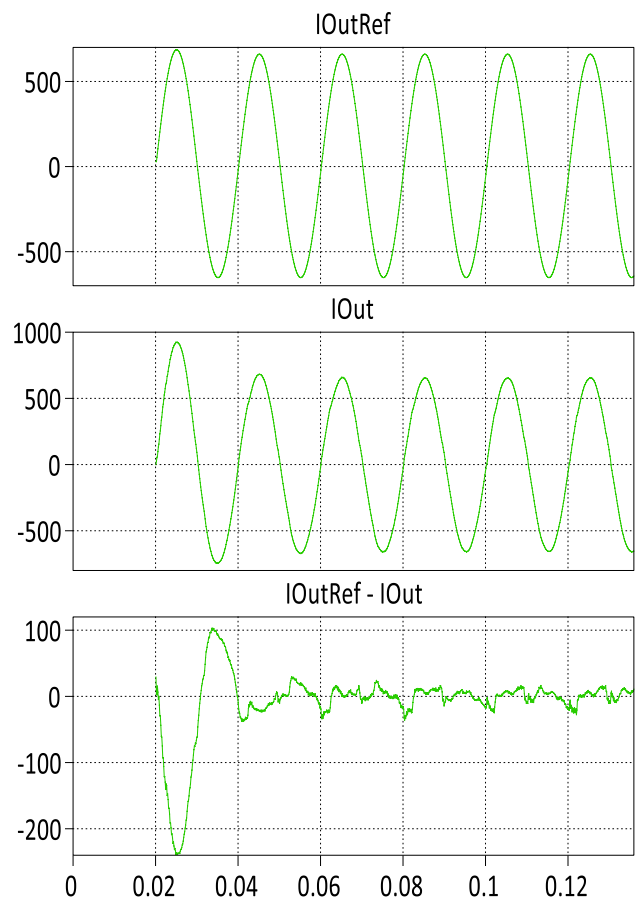


Fig. 11 Reference current, feedback current, and error current

Table 1 Error current—characteristics

	Current reference—feedback current
Maximum error value (instantaneous)	-240
Avg. steady-state error (for one cycle)	9

inverter voltage to match the grid voltage. In simulation, reference current is made to 5.4 kW, and the maximum overshoot is absorbed to be 46%. In practice, initial power delivered is limited and increases in step to reach the maximum rated power.

The inverter output voltage, output current, and output power at steady-state condition are shown in Fig. 18. In Fig. 18, RMS values of voltage, current, and power are taken to explain the stability of the inverter. From this figure, it has been observed that the RMS value of the voltage at steady-state condition is 230 V and the RMS value

of current at steady-state condition is 23.5 A and the RMS power is 5.4 kW. Multiplication of voltage and current values is observed from the graph shown in Fig. 18. The other simulation results are described in Table 3.

[

### 5 Experimental implementation and results

Experimental implementation of the current controller in the DC/AC converter circuits with LCL filter for a single-phase bidirectional inverter system is done and results

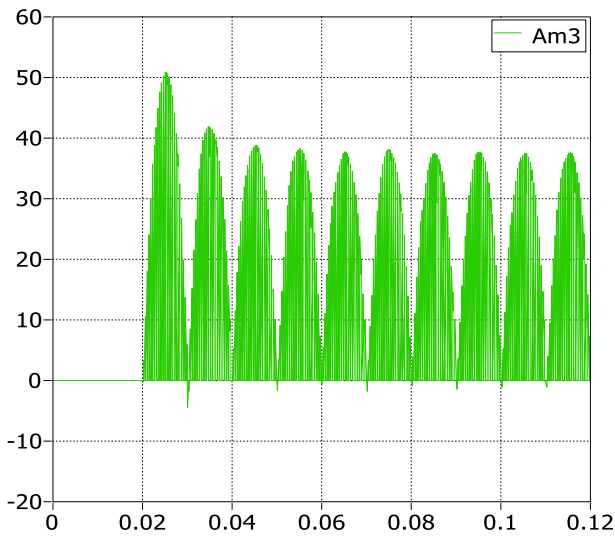


Fig. 12 Feedback current waveform observed from negative H-bridge

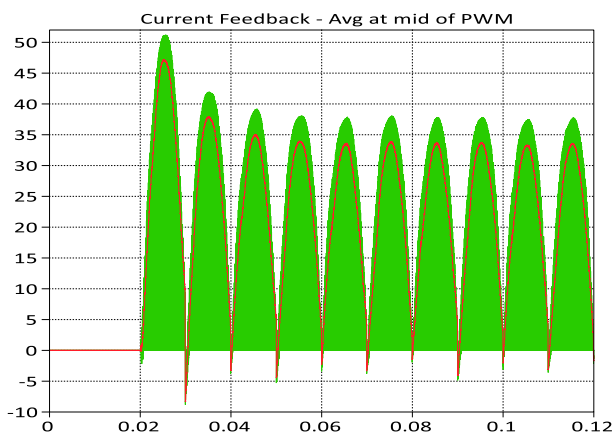


Fig. 13 Feedback and average current waveforms observed from negative H-bridge

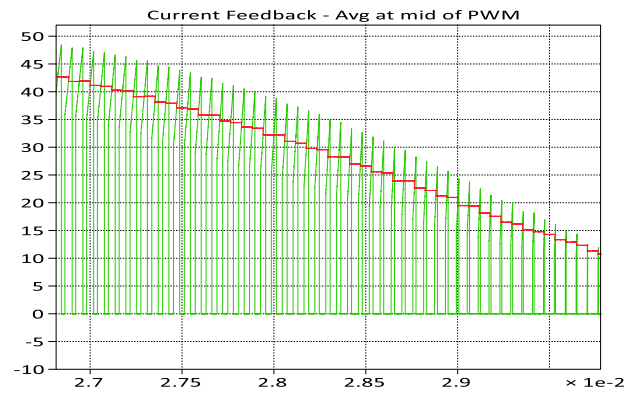


Fig. 14 Zoomed current waveform from negative H-bridge

are obtained. The proposed algorithm is implemented using 32-bit fixed-type TMS320F2812 DSP processor. The current controller reads the grid voltage, phase, frequency, and generates the electrical power based on the solar panel input power and DC link voltage. Inverter power is fed to the grid in phase with the grid voltage. H-bridge along with the filter converts the DC into AC specified by the grid parameters. STPOWER V channel 600 V IGBT suitable for solar inverter application is used as bridge. IGBT gates are driven by the PWM signals generated by DSP and isolated using gate drive optocoupler HCPL3120 which can source a minimum of 2A peak output current. Signal conditioning circuits are used to feed the DC voltage, inverter voltage/frequency, and the grid voltage/frequency to the DSP for feedback and control purposes. Also, the current through the power module and temperature of the power module have been measured by the DSP. ENS functionality is added using microcontroller. ENS monitors the grid voltage and frequency and controls the output relay which connects the inverter to the grid. ENS communicates with DSP through dedicated serial interface.

The current following through the H-bridge has been measured through a sense resistor of value 7.5mΩ. The voltage across 7.5mΩ has been amplified with a gain of ~8.15, which is then compared against the limit to disable the PWM signals during over current or reverse current flow.

PWM\_HALT, a halt signal, is activated when the current through the power modules exceeds 60A or when there is reverse current flow beyond 44A in the power modules. The output of the sensor is shown in Fig. 19.

The DC/AC inverter is based on an H-bridge converter as shown in Fig. 20. The output is connected to the utility in a single-phase configuration through an LCL filter.



Fig. 15 LCL filter circuit

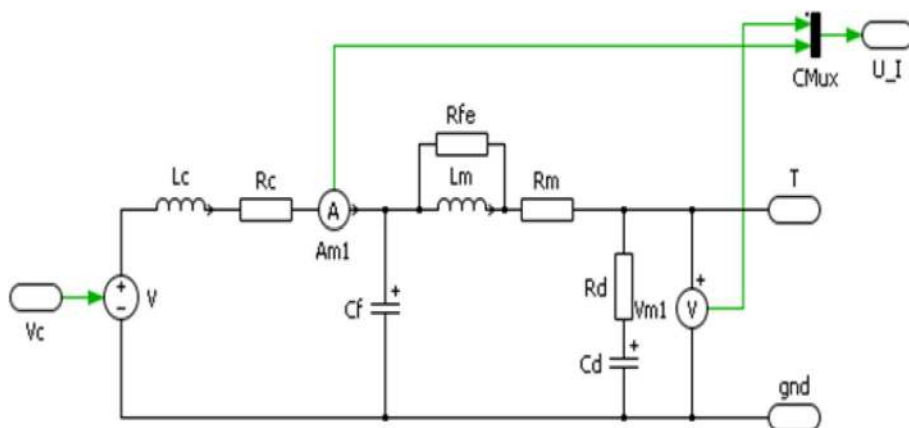


Fig. 16 Current control loop of LCL filter circuit

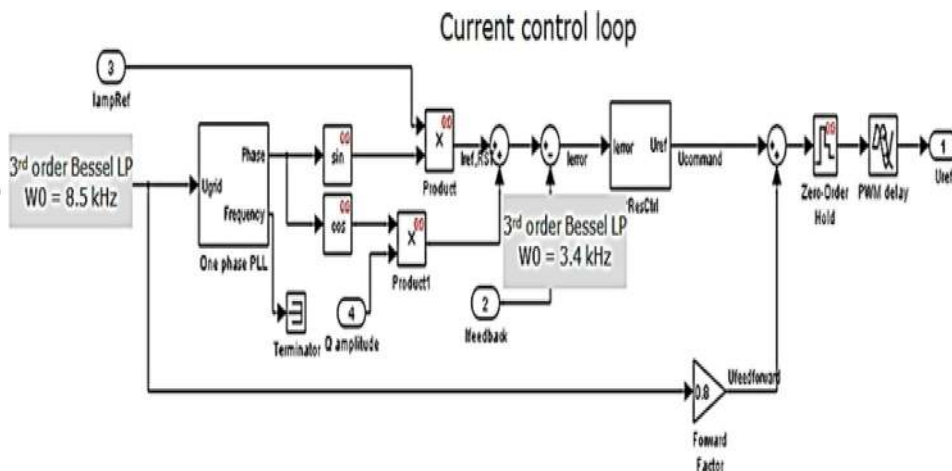


Table 2 LCL filter circuit parameters

Parameters	Values	Remarks
$L_c$	$330e^{-6}$	Nominal value
$R_c$	0.02	
$L_m$	$72e^{-6}$	Nominal value
$R_{fe}$	{inf, 200}	
$R_m$	0.008	
$C_f$	$10e^{-6}$	
$C_d$	$2.2e^{-6}$	
$R_d$	20ohm	

The switching frequency has been measured as 17 kHz. Gate drive signals of H-bridge circuit are shown in Fig. 21. Figure 22 shows the DC link voltage concerning the positive polarity of the input voltage. Voltage is measured

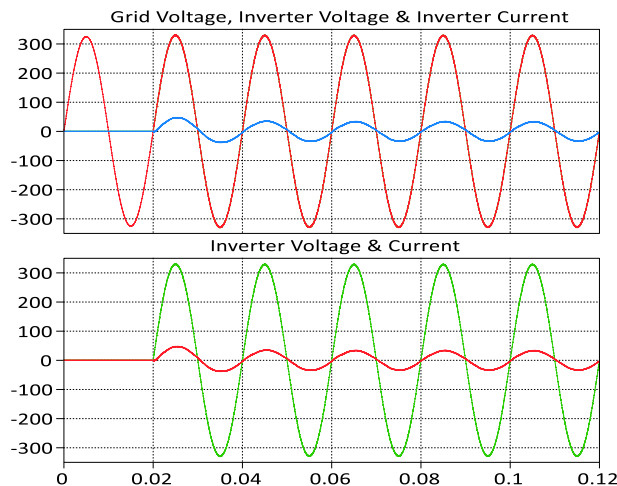


Fig. 17 Grid voltage and inverter output current

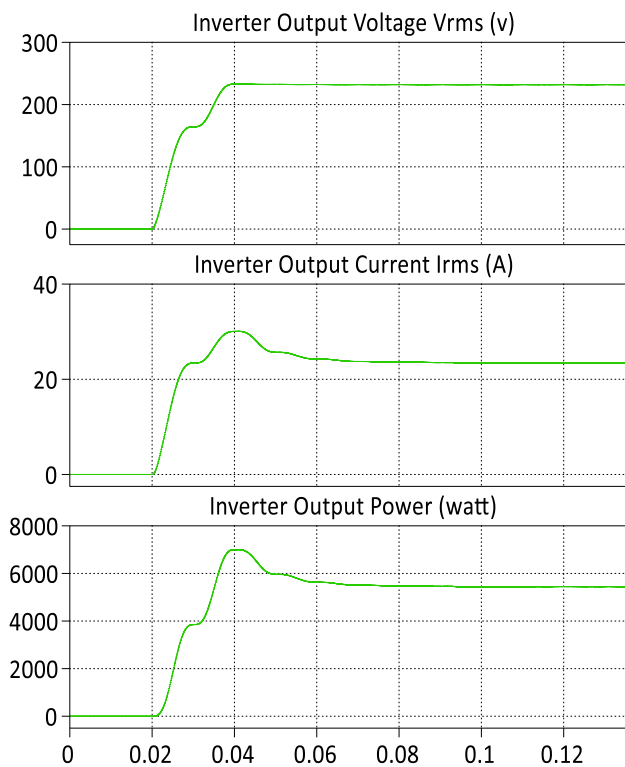


Fig. 18 Simulink output

Table 3 Simulation results for 5.4 kW inverter specification

Control parameters	Values
Current maximum overshoot	47 A (peak)
Current MOP%	42%
Settling time	2 cycles
Steady-state error	0.45 A (Avg.)

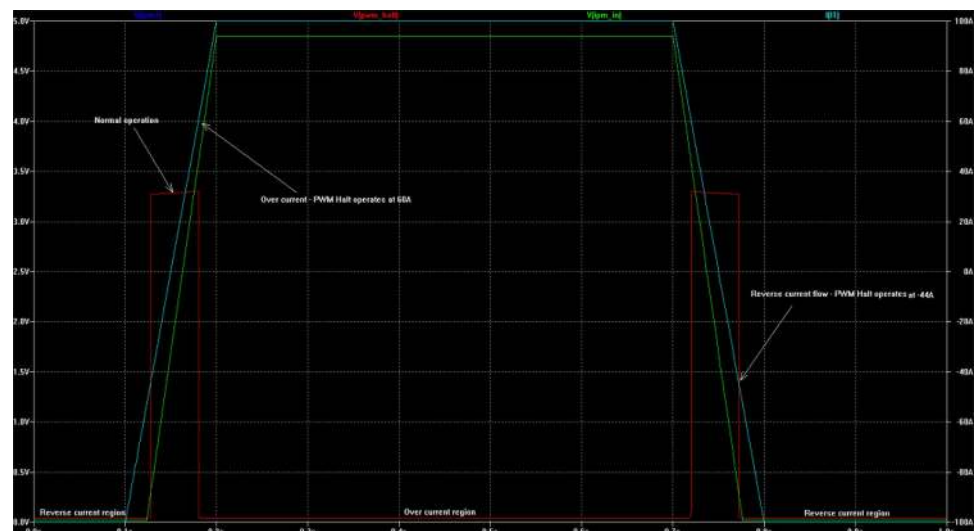
from the experimental setup and then it was plotted. The inverter output is connected to the grid utility through LCL filter in a single-phase configuration. Table 4 shows the LCL filter parameters and the parameters of the grid and inverter used for the experimental setup. The power flows in bidirectional mode that is to and from the grid to regulate the grid voltage at PCC (Point of Common Coupling). Fig. 23 illustrates distortion data received from spectrum analyzer; the THD% magnitude of the fundamental grid current injected into the grid is around 1.95% by employing PR controller, harmonic compensator, and LCL filter. The injected distortion in the grid current is well below IEEE 1547 Standards.

The resonance of the filter is dampened by suitably choosing the LCL parameter in the control loop circuit and stability margin is considered for resonance frequency.

Experimental results are shown in Figs. 24, 25, and 26 which depicts voltage and current waveforms captured when the inverter is connected to the grid along with LCL filter. Voltage and current of the grid are observed using PR controller for different values of pick to pick current. It is clearly observed that grid voltage and current closely matches the estimated voltage and current of the model with high tracking capability and zero steady-state error. Ripple attenuation of the grid current gets much better with proper tuning of LCL filter. It is also evident that the percentage of harmonics in the grid current is within limits of grid code standards at different current values (Fig. 27).

The stability of the LCL filter has also been tested by designing the control loop of the filter and further tested the stability margin with an ideal damping resistor value. Stability analysis of the LCL filter is done and the results are obtained. Figure 26 shows the Bode plot of the LCL filter where phase and magnitude are plotted. At

Fig. 19 PWM\_HALT signal and current sense waveforms



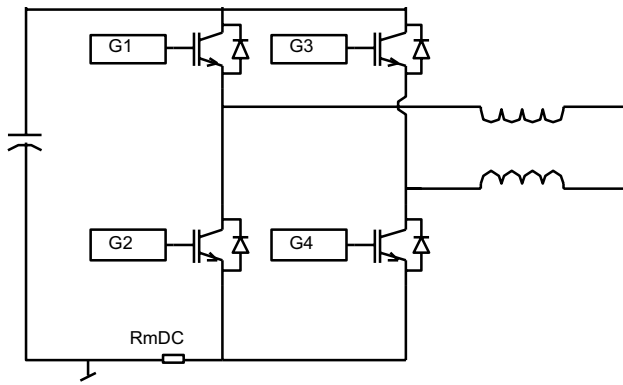


**Fig. 20** H-bridge of DC/AC board

$L_{grid} = 325\text{mH}$ , the FF closed loop has a large gain and at the same time a  $180^\circ$  phase shift. Experimental test setup of the solar inverter is shown in Fig. 28a, b.

## 6 Conclusion

DC/AC inverter circuit is modeled and simulated in this paper. Analysis has been carried out with detailed circuit design. Simulink model for the current control algorithm is designed for 5.4 KW with certain limitations in the model. Detailed circuit design and analysis have been carried out in this paper and the proposed design is validated. The proposed model describes the procedure and control strategy of current controller with output filter for single-phase two-directional grid-connected inverter system. To mitigate the switching ripple distortion to the grid, the filter parameters were carefully selected. It is observed that the inverter output with the proposed current controller with filter has better tracking capabilities, less ripple injected to grid, zero steady-state error, and strictly adheres to the grid code standard. The distortion is well below 5%. The model needs to be enhanced for additional analysis like the ride-through and effect of changes in grid impedance.

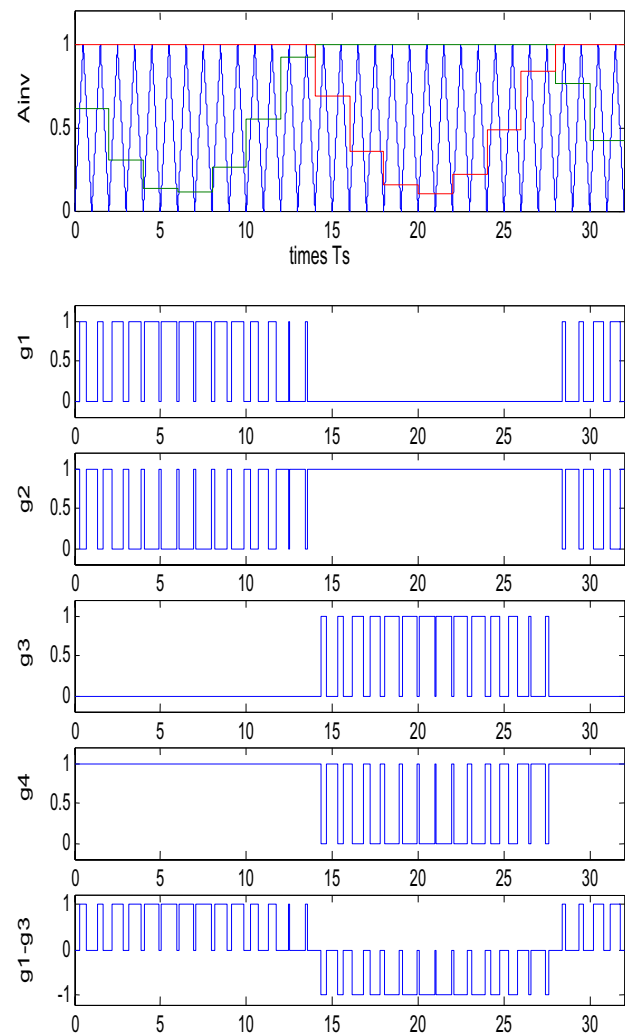


**Fig. 21** Gate drive signals of H-bridge

**Fig. 22** DC link voltage as measured and plotted



**Table 4** LCL and system parameter

Filter LCL	$L_{inv} = 72e^{-6}H, L_g = 330e^{-6}H, C_f = 10e^{-6}$
DC- input voltage	350–425 vdc
Switching frequency	17kHz
Inverter input DC voltage	400 V
Inverter output voltage	160 V –270 V rms AC
Inverter output frequency	47 Hz –53 Hz
Grid voltage at PCC	230 V
Grid frequency at PCC	50 Hz
Grid side inductance	.035mH
Grid resistance	0.1 $\Omega$

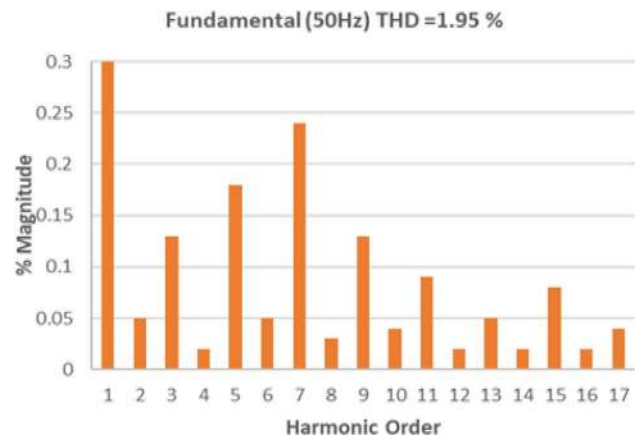


**Fig. 23** Harmonic order of the grid current injected

**Fig. 24** Voltage and current waveforms measured from inverter circuit

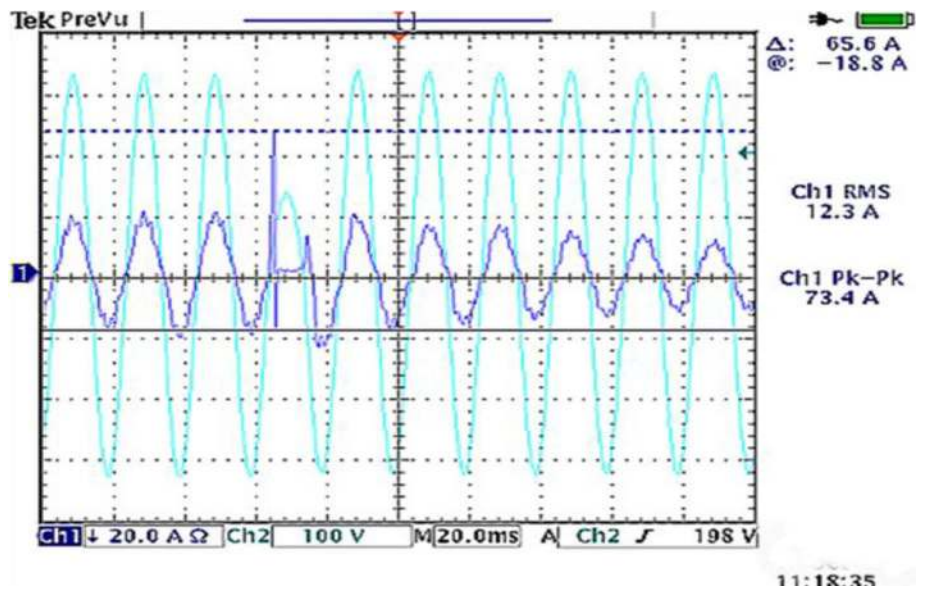


**Fig. 25** Experimental voltage and current waveforms from DC/AC circuit

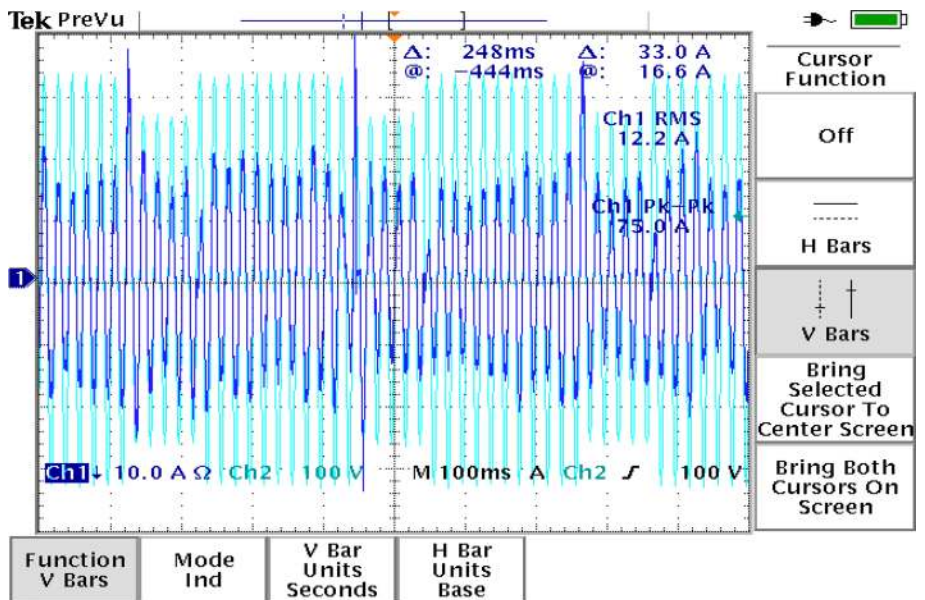




Fig. 26 Voltage and current waveforms from DC/AC circuit

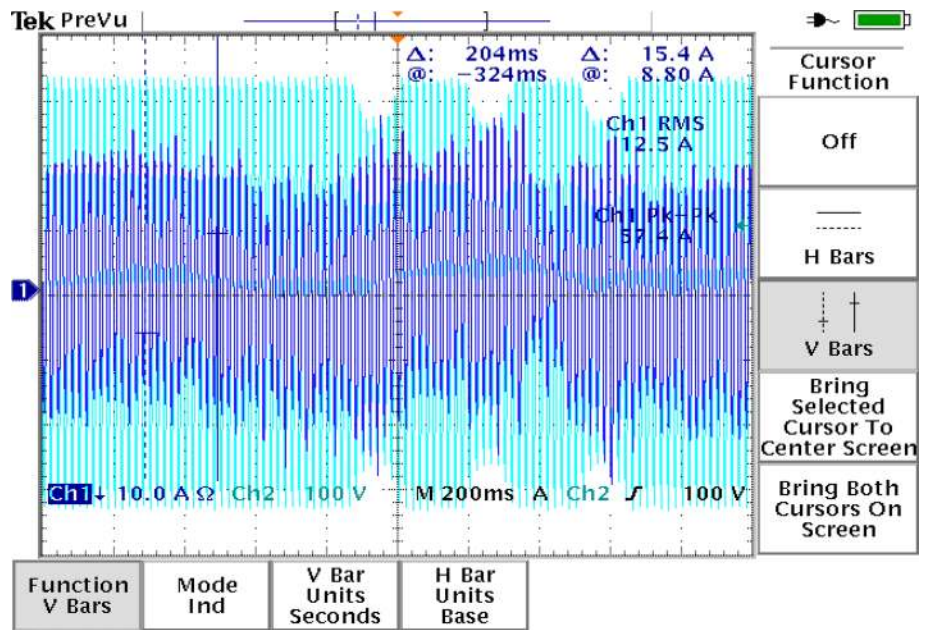
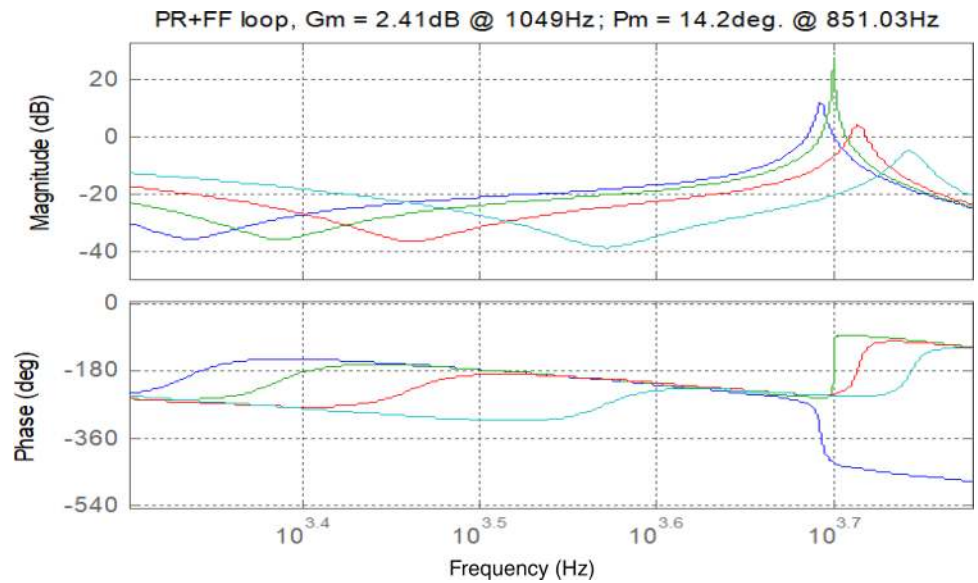
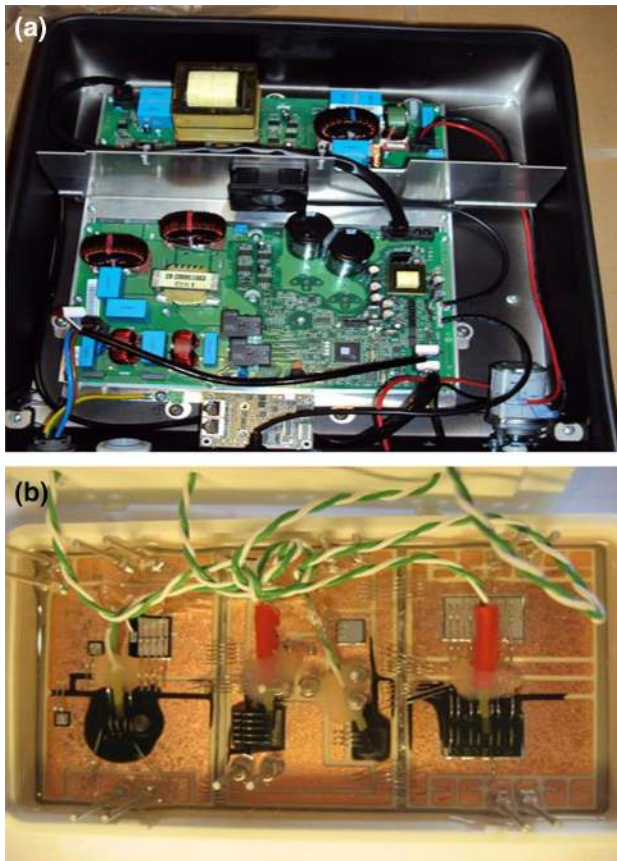


Fig. 27 Bode plot for LCL filter







**Fig. 28** **a** Experimental test setup of solar inverter. **b** DC/AC inverter module in experimental setup

**Acknowledgements** The authors gratefully acknowledge the Support of Department of Electrical Engineering, University of Technology and Applied Science (Oman), and AMU (India) for providing laboratory equipment and resources.

**Author contributions** Ayaz Ahmad conducted the research and simulation under the joint supervision of Dr. Rajaji L. & Dr. A. Iqbal. Dr. Rajaji L. and Dr. A. Iqbal did the analysis part. Dr. Rajaji L. and Ayaz Ahmad have performed data processing. All authors together prepared the manuscript.

**Data availability** Data and machines/equipment are available. MATLAB/SIMULINK model is available and can be shared on request.

### Compliance with ethical standards

**Conflict of interest** The authors declare no competing interests.

**Open Access** This article is licensed under a Creative Commons Attribution 4.0 International License, which permits use, sharing, adaptation, distribution and reproduction in any medium or format, as long as you give appropriate credit to the original author(s) and the source, provide a link to the Creative Commons licence, and indicate if changes were made. The images or other third party material in this article are included in the article's Creative Commons licence, unless

indicated otherwise in a credit line to the material. If material is not included in the article's Creative Commons licence and your intended use is not permitted by statutory regulation or exceeds the permitted use, you will need to obtain permission directly from the copyright holder. To view a copy of this licence, visit <http://creativecommons.org/licenses/by/4.0/>.

### References

- Vijayakumari BR, Warriar and N Devarajan (2014) Topologies and control of grid connected power converters International Conference on Circuits, Power and Computing Technologies [ICCPCT-2014], Nagercoil, pp. 401–410,
- Rhili H, Trabelsi and Hmad J (2019) PI and PR current controllers of single phase grid connected PV system: analysis, comparison and testing. 16th International Multi-Conference on Systems, Signals & Devices (SSD), Istanbul, Turkey, 2019, pp. 700–705, doi: <https://doi.org/10.1109/SSD.2019.8893232>.
- Daniel Zammit, Cyril Spiteri Staines, Maurice Apap, John Licari. (2017) Design of PR current control with selective harmonic compensators using Matlab. Journal of Electrical Systems and Information Technology, Volume 4, Issue 3, Pages 347–358, ISSN 2314–7172, <https://doi.org/https://doi.org/10.1016/j.jesit.2017.01.003>.
- Yaosuo Xue, Liuchen Chang, Sren Baekhj Kjaer, J. Bordonau and T. Shimizu (2004) Topologies of single-phase inverters for small distributed power generators: an overview in IEEE Transactions on Power Electronics, vol. 19, no. 5, pp. 1305–1314
- Teodorescu R, Blaabjerg F, Borup U, Liserre M (2004) A new control structure for grid-connected LCL PV inverters with zero steady-state error and selective harmonic compensation Nineteenth Annual IEEE Applied Power Electronics Conference and Exposition, APEC '04., Anaheim, CA, USA, 2004, pp. 580–586 Vol.1.
- Sharaf AM, Haque ARNMRU (2005) Low cost utility interconnected photovoltaic scheme for residential/ village/ cottage electricity Proceedings of the Thirty-Seventh Southeastern Symposium on System Theory, 2005. SSST '05. Tuskegee, AL, USA, pp. 435–438.
- Park K, Seo B, Jo K, Heo J, Kim H and Nho E (2019) Current Controller Design of a Grid Connected Inverter Using LCL Filter. 2019 10th International Conference on Power Electronics and ECCE Asia (ICPE 2019 - ECCE Asia), Busan, Korea (South), pp. 2356–2361.
- Chhabra M, Barnes F (2014) Robust current controller design using mu-synthesis for grid-connected three phase inverter. 2014 IEEE 40th Photovoltaic Specialist Conference (PVSC), Denver, CO pp. 1413–1418,
- Xiu'e Su, Keliang Zhou, Wenjie Zhu, Li Zhu (2010) Proportional-resonant current control of single-phase grid-tied PV inverter system Proceedings of the International Conference on Electricity Distribution, China, pp.1 – 4.
- Dasgupta S, Mohan SN, Sahoo SK, Panda SK(2011) A Lyapunov function based current controller to control active and reactive power flow in a three phase grid connected PV inverter under generalized grid voltage conditions Proceedings of the IEEE 8th International Conference on Power Electronics and ECCE Asia , pp. 1110 – 1117
- Dasgupta S, Sahoo SK, Panda SK (2010) A novel current control scheme using Lyapunov function to control the active and reactive power flow in a single phase hybrid PV inverter system connected to the grid Proceedings of the IEEE International Conference on Power Electronics Conference , pp. 1701 – 1708

12. Dasgupta, S, Mohan SN, Sahoo SK, Panda SK (2011) Derivation of instantaneous current references for three phase PV inverter connected to grid with active and reactive power flow control Proceedings of the IEEE International Conference on Power Electronics Conference pp.1228 – 1235
13. Hattori N, Morotomi N, Miyake S, Nakaoka M (2010) Utility grid-tied 3-phase central PV inverter embedding neutral point voltage shifting principle into instantaneous current control implementation Proceedings of the International Conference on Power Electronics , pp. 3230 – 3235
14. Vazquez G, Rodriguez P, Ordonez R, Kerekes T, Teodorescu R(2009) Adaptive hysteresis band current control for transformerless single-phase PV inverters Proceedings of 35th Annual Conference of IEEE Industrial Electronics, pp. 173 – 177
15. Selvaraj J, Rahim NA, Krismadinata C (2008) Digital PI current control for grid connected PV inverter Proceedings of the 3rd IEEE Conference on Industrial Electronics and Applications, pp. 742 – 746
16. Kahrobaeian A, Farhangi S (2010) Stationary frame current control of single phase grid connected PV inverters Proceedings of the International Conference on 1st Power Electronic & Drive Systems & Technologies, pp. 435 – 438
17. Bo Yang, Jiande Wu, Xiaodong Lu, XiangningHe (2008) An improved DSP-based control strategy with predictive current control and fuzzy voltage control for grid-connected voltage source inverters Proceedings of the 34th IEEE Annual Conference on Industrial Electronics pp. 2296–2300
18. Mohan N, Undeland T M, Robbins W P (2003) Power electronics: converters, applications and design 3rd edition, John Wiley & Sons, Inc, ISBN: 0–471–58408–8
19. Martins D. C, Demonti R (2002) Grid connected PV system using two energy processing stages Proceedings of the IEEE 29th photovoltaic specialists conference, IEA, pp. 1649–1652
20. Shimizu T, Wada K, Nakamura N (2006) Flyback-type single-phase utility interactive inverter with power pulsation decoupling on the dc input for an AC photovoltaic module system. IEEE Trans Power Electron 21(5):1264–1272
21. Turitsyn K, Sulc P, Backhaus S, Chertkov M (2011) Options for control of reactive power by distributed photovoltaic generators. Proceedings of IEEE 99(6):1063–1073
22. Vazquez G, Rodriguez P, Ordonez R, Kerekes T, Teodorescu R (2009) Adaptive hysteresis band current control for transformerless single-phase PV inverters Proceedings of 35th Annual Conference of IEEE Industrial Electronics, pp. 173 – 177
23. Dong Mi, Luo An, BaiLisha, Yang Jian (2007) An integrative control scheme for boost-buck inverter in grid connected photovoltaic systems Proceedings of the IEEE International Conference on Twenty Second Annual- I Applied Power Electronics, pp. 524 – 528
24. Vongmanee V (2002) The vector control inverter for a PV motor drive system implemented by a single chip DSP controller ADMC331 Proceedings of the Asia-Pacific Conference on Circuits and Systems, pp. 447 – 451
25. Al-Saedi W, Lachowicz SW, Habibi D (2011) An optimal current control strategy for a three-phase grid-connected photovoltaic system using particle swarm optimization Proceedings of the IEEE International Conference on Power Engineering and Automation (PEAM), Vol. 1, pp. 286 – 290,.
26. Nousiainen L, Puukko J, SuntioT (2011) Appearance of a RHP-zero in VSI-based photovoltaic converter control dynamics Proceedings of the - IEEE 33<sup>rd</sup> International Telecommunications Energy Conference, pp. 1 – 8
27. Husev O, Roncero-Clemente C, Makovenko E, Pimentel SP, Vinnikov D, Martins J (2020) Optimization and implementation of the proportional-resonant controller for grid-connected inverter with significant computation delay . IEEE Trans Industr Electron 67(2):1201–1211
28. Xu J, Qian Q, Zhang B, Xie S (2019) Harmonics and stability analysis of single-phase grid-connected inverters in distributed power generation systems considering phase-locked loop impact in IEEE transactions on sustainable. Energy 10(3):1470–1480
29. Nazeri AA, Zacharias P, Ibanez FM, Somkun S (2019) Design of proportional-resonant controller with zero steady-state error for a single-phase grid-connected voltage source inverter with an LCL output filter. IEEE Milan Power Tech Milan Italy 2019:1–6. <https://doi.org/10.1109/PTC.2019.8810554>

**Publisher's Note** Springer Nature remains neutral with regard to jurisdictional claims in published maps and institutional affiliations.